Experimental and Numerical Impact Responses of an Innovative Rockfall Protection Structure Made of Articulated Concrete Blocks

Agathe Furet, Pascal Villard, Jean-Philippe Jarrin, Stéphane Lambert

Rock Mechanics and Rock Engineering
https://doi.org/10.1007/s00603-022-02957-x

ORIGINAL PAPER

Experimental and Numerical Impact Responses of an Innovative Rockfall Protection Structure Made of Articulated Concrete Blocks

Agathe Furet[1,2,3] · Pascal Villard[3] · Jean-Philippe Jarrin[1] · Stéphane Lambert[2]

Received: 9 December 2021 / Accepted: 31 May 2022

Abstract

This study deals with an innovative type of protection structure for gravity-driven natural hazards such as landslides (slope failures, rockfalls, etc.) consisting of a vertical wall made up of interconnected concrete blocks. This type of articulated structure presents many advantages including reduced footprint, versatility and easy maintenance. The response of such a structure under impact is investigated considering projectiles with kinetic energies of 520 and 1020 kJ, based on real-scale impact experiments and numerical simulations. The finite difference model is described in detail as well as the experiments. The model was developed focusing on the global structural impact response while keeping the computation time reasonable. The model parameter calibration is based on data in the literature and complemented with specific measurements. The experimental data allows us to describe the impact response of the structure and identify the main mechanisms controlling this response (sliding, tilting, and fracturing). The simulation results revealed that the model is efficient in mimicking this response, in terms of deformation amplitude and evolution with time. Finally, the numerical model made it possible to highlight complex mechanisms that were not possible to experimentally determine such as the different energy dissipation modes within the wall.

Highlights

- Full-scale impact experiments demonstrating the impact strength of articulated walls made of concrete blocks and metallic elements up to 1000 kJ.
- Finite difference model of the structure validated against experimental data.
- Highlights of the prevailing mechanisms involved in the impact response of the structures based on both numerical and experimental investigations.
- Based on simulation results, friction between concrete blocks and damage to concrete contribute up to 70% of the projectile kinetic energy.

✉ Agathe Furet
agathe.furet@geolithe.com

Pascal Villard
pascal.villard@univ-grenoble-alpes.fr

Jean-Philippe Jarrin
jp.jarrin@geolithe.com

Stéphane Lambert
stephane.lambert@inrae.fr

[1] Géolithe, 181 rue des Bécasses, 38920 Crolles, France

[2] Univ. Grenoble Alpes, INRAE, ETNA, 38000 Grenoble, France

[3] Univ. Grenoble Alpes, CNRS UMR 5521, Grenoble INP, 3SR, 38000 Grenoble, France

Published online: 12 July 2022

Keywords Rockfall-protective structure · Boulder impact · Numerical modeling · Finite difference method · Real-scale experiments

List of symbols

C	Cohesion
ds_i	Cumulative shear displacement component in axis i
$\Delta z\text{min}$	Smallest dimension in the normal direction of the two zones in contact
ΔE_i	Energy dissipated by friction at node i, at current time
E_{fric}	Energy dissipated by friction
f^s	Mohr–Coulomb failure criterion
f^t	Tension cutoff criterion
Fs_i	Instantaneous shear force component in axis i
G	Shear modulus
K	Bulk modulus
$k_{\text{criterion}}$	Stiffness criterion for interfaces
Φ	Friction angle
σ_i	Principal stresses i
σ^t_{max}	Tensile strength applied in the model
σ^t	Tensile strength

1 Introduction

Massive vertical structures such as embankments are often used to protect infrastructure and people from rockfall (Lambert and Bourrier 2013). These structures are generally located in zones with space constraints due to the site topography and the distance to the infrastructures to protect (Simmons et al. 2009; Colgan and Ewe 2019). In such situations, the structure footprint can be reduced increasing the facing steepness, for example using rip-rap at the facing or internal reinforcement. Both these adaptations have an influence on the embankment response to impact, which depends on dynamic effects that have to be accounted for in the design (Peila et al. 2007; Lambert et al. 2014; Korini et al. 2019). In this context, several studies have addressed the impact response of structures optimized in size based on full-scale experiments. Hearn et al. (1996) have demonstrated that rectangular in cross-sectional structures 3.1 m in height and 1.8 m in width at the base could resist a 1400 kJ impact. The reinforced embankments tested by Peila et al. (2002), with isosceles cross sections, 4.8 m in height and 5 m in width at the base, were demonstrated to be able to arrest blocks with a 4500 kJ kinetic energy. Hara et al. (2012) verified that the so-called piled geo-wall, 2 m tall with total footprint of 1.3 m, is able to stop a 100 kJ kinetic energy projectile. Lambert et al. (2020) compared the response of different sandwich structures made of geocells, 4 m in height and 3 m in width at the base, and showed that this type of structure withstands 2000 kJ kinetic energy impacts. Korini et al. (2021) showed that 1/3 reduced-scale slender reinforced bunds, 2.4 m in height for a 1.25 m base width, could withstand a 170 kJ impact with very small deformation. In parallel, numerical models have been developed using the provided experimental data for calibration and validation purposes (Peila et al. 2002, 2007; Ronco et al. 2009; Breugnot et al. 2016).

Increasing urbanization intensifies the space limitations and requires easy to build, maintain and repair protection structures with reduced footprints. As an improved alternative to embankments, structures integrating concrete components have been recently proposed to answer this demand. Green and Finlan (2021) have validated the performance of a modular sandwich structure 2 m wide and 3 m high. It consists of layers made up of gabion cages filled with sand for the intermediate layer and stones for the front face layer, leant against a wall made up of stacked precast concrete blocks, reinforced vertically with steel bars. The authors performed tests at 250 kJ and 750 kJ energies, at two impact heights (1.5 m and 2.25 m) to address the structure stability vs. sliding and tilting. The results showed that despite a high penetration in the gabions, downstream movements remain limited and do not cause the failure of the structure. Based on the evidence that design methods considering estimates of the contact force led to concrete structure oversizing, by underestimating inertial effects and energy losses, Lam et al. (2018) and Yong et al. (2019) studied the impact response of rigid concrete walls. The first addressed the rotation of slender walls (Lam et al. 2018) and the second addressed the sliding of L-shaped walls (Yong et al. 2019). Experimental works, complemented with (finite element method) simulations, led the authors to propose analytical methods based for the coefficient of restitution to take into account dynamic effects (inertia, energy dissipation) that occur during impact.

The present article deals with articulated structures constructed from prefabricated concrete blocks linked together thanks to structural metallic elements. This type of protective wall presents the advantages of moderate footprint, modularity, versatility, ease of construction, as well as reduced maintenance and repair costs (Lorentz et al. 2018). Its development was based on numerical modeling and experiments on small and full-scale structures. Impact tests performed on small-scale simple articulated walls of various geometries and configurations (Furet et al. 2020) evidenced the main mechanisms associated with the dynamic response of such walls: sliding at the base, relative displacement between the blocks in the horizontal and vertical directions, and tilting of the wall inducing uplift on the structure front side. All these mechanisms give the structure an ability to deform without reaching failure, thus increase its capacity

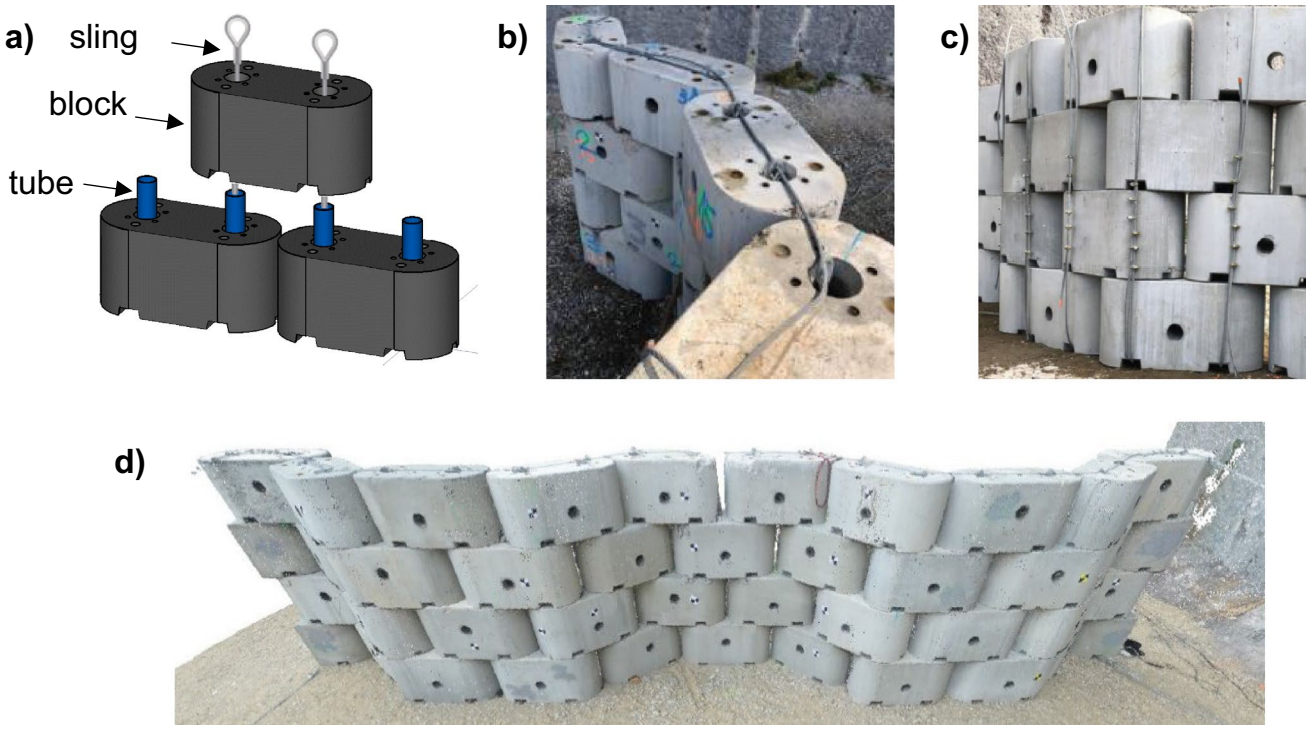

Fig. 1 Tested structure. **a** Main components of the Bloc Armé® structure, **b** structure crown, **c** cables forming a wire belt at the back of the structure, **d** A 3.2 m tall zigzag wall before impact

in withstanding the impact. A finite difference numerical model of a linear articulated wall, developed with the code FLAC3D (Itasca Consulting Group Inc. 2019) and validated against the experimental data, allowed us to quantify the energy dissipated during the impact by the various mechanisms (Furet 2020).

This study focuses on the response of full-scale zigzag walls exposed to impacts with energies up to 1000 kJ. First, this article describes the structure, the experiments and the instrumentation. Then, the experimental results are presented focusing on the dynamic and final deformation of the walls. The numerical model is exposed with the detailed description of the parameters. Finally, numerical results are (i) compared to experimental results to demonstrate the ability of the model to reproduce the real structure behavior under impacts and (ii) further elaborated to address the involved phenomena, in particular concerning energy dissipation.

2 Full-Scale Impacts Experiments on Walls

2.1 Structure

The structure consists of concrete blocks that are piled up in staggered rows and, in an innovative way, linked together by an assembly of metallic tubes, cables and slings (Fig. 1). The innovation also lies in the slack given to the structure and resulting from the space left between tubes and concrete blocks, on one side, and between adjoining concrete blocks on the other. The metallic elements ensure a mechanical continuity along the horizontal and vertical axis, allowing the structure to behave as a single but deformable body. This design favors forces distribution within the structure, increases the mass associated with the structure impact response, while limiting the development of high impact forces associated with the use of concrete elements. Based on this concept and depending on the site configuration and impact energy, structures of various shapes and configurations (linear, zig-zag, with or without buttress…) may be designed and easily implemented, with a footprint from 0.8 m to a few meters.

In this study, a zigzag wall is considered. This configuration has the advantage of offering a structure with an higher overturning stability than a linear wall, with limited increase in footprint. This is related to the fact that the zig-zag configuration gives the structure higher deformation capacities, resulting from its unfolding. This configuration aimed at allowing the wall to resist impacts exceeding 1000 kJ in energy.

The experiments concerned two zigzag walls, 3.2 m in height and 14 m in length, made up of 38 blocks and four half-blocks stacked in four rows (Fig. 1a, b, c and d).

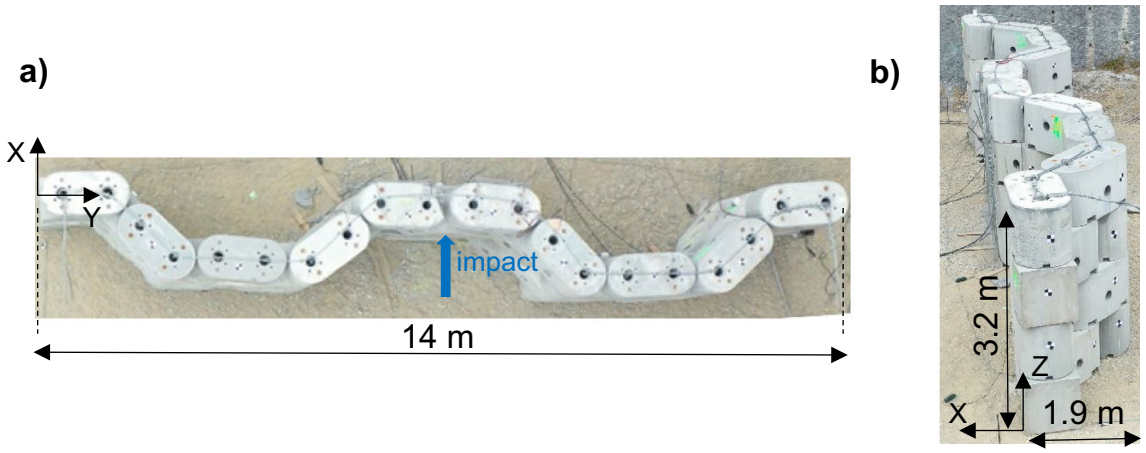

Fig. 2 **a** Top and **b** side view of a wall before impact also showing the three reference axes

The blocks were made from C35/45 concrete reinforced with internal rebars. The blocks dimensions were 0.76*1.56*0.8 m (width*length*height), resulting in a mass of 2000 kg. Each block was equipped with two vertical holes, 154 mm in diameter, to receive 140 mm in external diameter metallic tubes (Fig. 1a). The free space around the tubes was thus 7 mm. A sling was inserted in each tube along the vertical axis, from the base to the crown of the structure. The extremities of the slings were blocked by a steel bar at the base and by a cable running along the structure crown (Fig. 1b). Once installed, the average free space between two adjoining blocks was 40 mm. The structure was equipped with six extra cables to form a belt, circling the blocks in the impact vicinity (Fig. 1c).

2.2 Impact Tests Description

The experiments consisted in sub-horizontal impacts by a reinforced concrete projectile on the structure shown Figs. 1 and 2. The projectile shape was in accordance with the requirements in view of impact tests on flexible barriers (EOTA 2018), with a size of 1.1 m and a mass of 2600 kg. The experiments were performed on the pendulum testing facility of the Université Gustave Eiffel test site (Montagnole, France) allowing us to control the impact position and constrain the incidence angle and rotation to zero.

Two identical walls were submitted to one impact test each, with a projectile kinetic energy of 520 and 1020 kJ for the first and second tests, respectively (Table 1). In both cases, the block impacted the structure at its mid-length with near nil rotation velocity and inclination. After the first test, the wall was completely rebuilt with the same geometry. To reduce the damage to the structure during the second test, the concrete blocks in the impact vicinity were manufactured with a higher volume of rebars and additional internal welded wire mesh.

Table 1 Description of the two full-scale impact experiments

Impact $n°$	Impact height (m)	Incident angle (°)	Mass (kg)	Velocity (m/s)	Energy (kJ)
1	1.7	0	2600	20	520
2	1.7	0	2600	28	1020

In the following, the X-axis is oriented perpendicularly to the wall longitudinal axis in the horizontal plane, the Y-axis corresponds to the longitudinal axis of the wall and the Z-axis corresponds to the vertical axis.

2.3 Instrumentation

Various measurement techniques were used to describe the mechanical response of these walls under impact loading with the aim of addressing their dynamic behavior. A particular focus was placed on the wall displacement, considering that measuring stress and strain was technically difficult or even impossible and not relevant when dealing with a wall made of articulated rigid blocks.

Topographical surveys were conducted using drones and photogrammetric methods, to produce 3D models of the walls before and after each impact. It allowed us to describe the post-impact wall deformation in comparison with its initial geometry. This allowed us to determine the displacement with an accuracy of 20 mm, which is relatively precise considering the global displacement amplitude of the wall.

Two cameras filmed the impacts at a rate of 1000 frames per second from front and rear points of view. The rear camera is placed just behind the wall, at impact height and filmed horizontally, perpendicularly to the impact trajectory. The high-speed images of this camera were used to measure the displacement with time of various points of the wall during

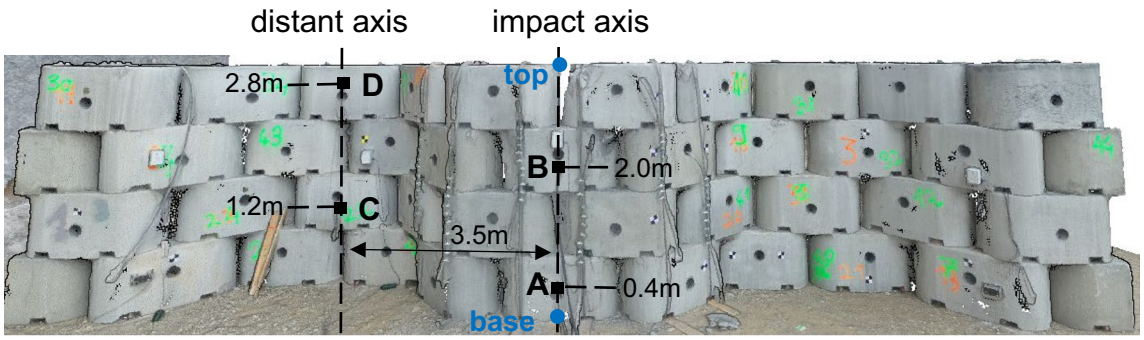

Fig. 3 Measure points of the wall, equipped with sensors (**A**–**D**) or pointed on high-speed camera images (base, top)

impact with an accuracy of a few centimeters. Nevertheless, this accuracy was lesser in some points, and in particular at the base of the wall, notably due to the reduction in visibility resulting from the projection of concrete fragments or dust.

The back face of the structure was equipped with different sensor types, installed in different locations, similarly to that in Lambert et al. (2020). First, measurements concerned points along a vertical axis at the structure mid-length, where impact occurs. Second, measurements also concerned points along a vertical axis 3.8 m in distance from the previous one. In the following, the former and latter axes are referred to as impact and distant axes, respectively. In addition, the planes defined by each of these axes and the X-axis are referred to as impact and distant planes (Fig. 3). In these points, piezo-resistive accelerometers, tiltmeters and the cable extremity of cable extension sensors were installed. These sensors provided synchronous full-time data measured with a 2 kHz data acquisition system. The impact beginning was defined from the acceleration measured at the closest distance from the impact point (point B). Unfortunately, many measures are not available, partial or not reliable. This is due to the extreme experimental conditions, inducing block fracturing and fragment projection on sensor cables for example. For this reason, the real-time measurements presented in the following are restricted to those taken at point B, 2.0 m from the ground on the impact axis, and point D, 2.8 m from the ground on the distant axis.

3 Experimental Results

3.1 General Observations

The walls successfully stopped the projectile for both the 520 kJ and the 1020 kJ impact experiments. The walls experienced large displacement and were damaged but did not collapse. The high-speed camera acquisition revealed similar trends in terms of global kinematics during the two impacts. To begin with, and for a very short period of time, only the impacted block moved. Then, blocks at the base and top of the wall in the impact axis started moving along the X-axis, and the wall experienced sliding with a slight uplift over total length of two blocks on both sides of the impact axis. Thereafter, blocks further away from the impact axis progressively moved, with a translation along the X- and Y-axis combined with rotation along the Z-axis. Small movements of the blocks were observed at the wall extremities. The wall progressively tilts on its rear edge from the moment when the base sliding stopped. This tilting remained small and decreased with the distance to the impact axis. Finally, the walls experienced a slight reverse displacement.

The blocks in contact with the projectile experienced damage during both experiments. The impacted block, in the wall center, was fractured along the two holes during the 520 kJ impact. Also, spalls were observed in different locations and were attributed to friction at the contact points between superimposed blocks. During the second impact, the impacted block disintegrated, even though it was reinforced compared to that in the first experiment. The blocks at the second row in the impact axis also broke. The large fragments generated were contained by a double-twisted mesh, placed for this purpose, on the back face of the wall. The mechanical continuity of the wall was maintained in spite of this damage, thanks to the metallic reinforcement.

3.2 Final Deformation and Displacement

In addition to the previous observations, the photogrammetric 3D models revealed a wall displacement over a length of three blocks on both sides of the impact axis after the first impact and eight blocks after the second impact (Figs. 4 and 5). Close to the impact axis, blocks in the first and third rows from the base experienced translation along the X-axis and blocks in the second and fourth rows from the base experienced translation in both the X- and Y-axis, combined with

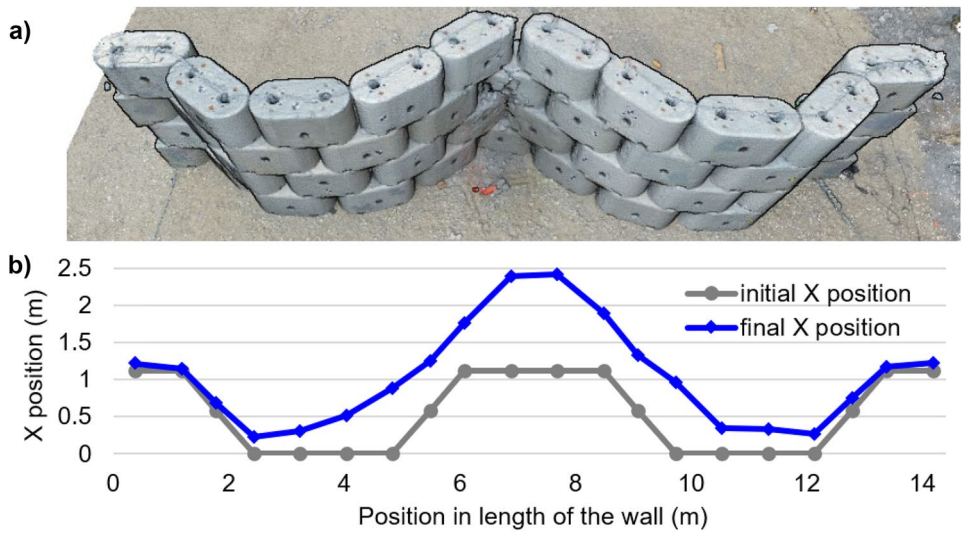

Fig. 4 View of the wall after the 520 kJ impact, **a** total deformation, **b** positions of the holes of the blocks before (initial) and after (final) impact

rotation along the Z-axis. Blocks at distance from the impact axis experienced the same type of displacement as the latter. No residual displacement is observed at the wall extremities.

Contrary to these global trends, the wall deformation magnitude differed between the two experiments. The X-axis residual displacement at the top of the wall on the impact axis reached 0.87 m and 1.42 m for the first and second experiments, respectively (Table 2). A difference in amplitude was also observed on the distant plane between the two experiments, with smaller values and with the same order of magnitude along the X- and Y-axes. Globally, the residual displacement was lower at the wall base in comparison with the top, revealing inclination of the wall.

Experiments showed that the criterion concerning the downhill deformation in comparison to the mid-height width proposed by Lambert and Kister (2018) for rockfall protection embankment is not appropriate for these articulated structures. The walls withstand the impacts with a deformation exceeding the threshold of 25% of their width and neither damages to the components nor geometry changes suggest that the structure is close to failure.

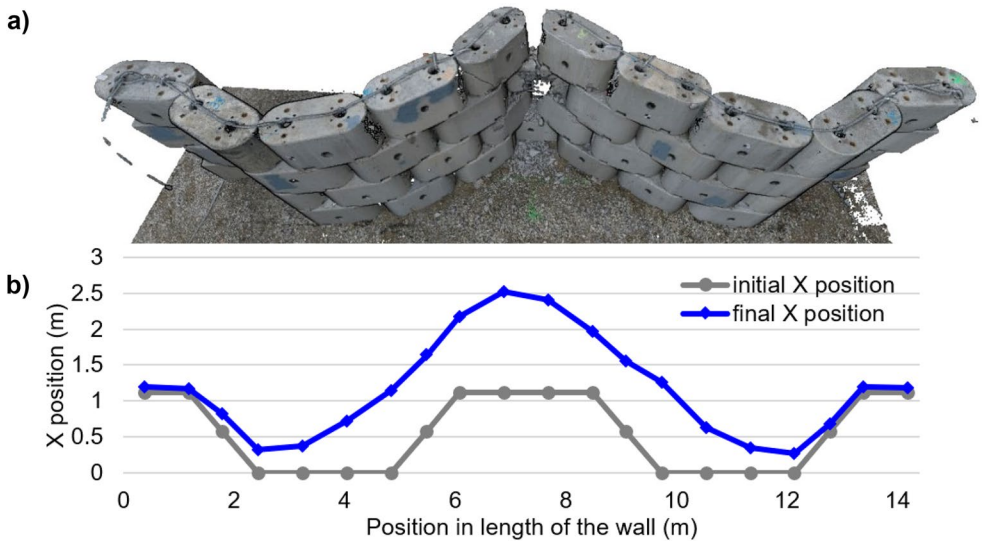

Fig. 5 View of the wall after the 1020 kJ impact, **a** global deformation, **b** positions of the reservations before (initial) and after (final) impact

Table 2 Residual displacement along the X-axis (3d photogrammetric data) (m)

Impact	Impact axis		Distant axis	
	Base	Top	Base	Top
1: 520 kJ	0.72	0.87	0.10	0.11
2: 1020 kJ	1.00	1.42	0.33	0.40

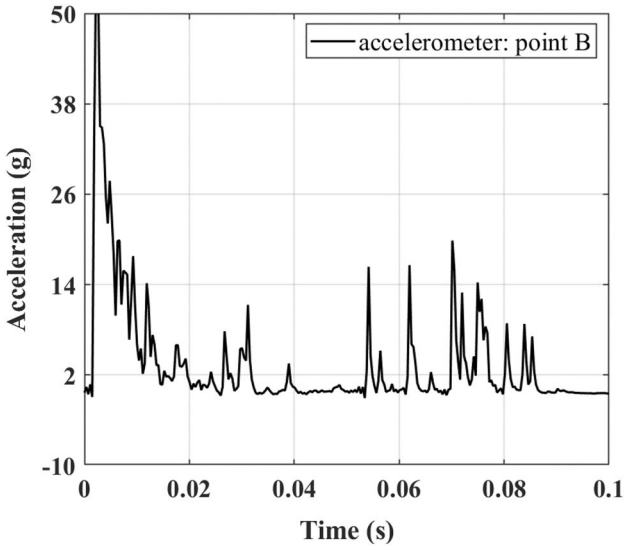

Fig. 6 Acceleration of the impacted block (point B) during the 520 kJ impact experiment

3.3 Dynamic Response of the Wall

The acceleration measured at the rear of the impacted block indicates that during the first experiment (520 kJ), the impact lasted less than 0.02 s, with a peak value exceeding 50g (Fig. 6). After 0.02 s, the contact force between the projectile and the impacted block is very small to nil, suggesting that both move at the same velocity or that the contact is lost. The multiples small amplitude peaks observed later on are attributed either to short duration projectile–block contacts or to the interaction of the impacted block with the other blocks of the wall. This measurement is not available for the second experiment.

High-speed camera images reveal that the displacement of the wall along the X-axis increases linearly with time, slows down before reaching a maximal value, decreases and then stabilizes (Fig. 7). The reverse displacement is significant at the top of the wall and smaller at its base (Table 3). The residual values are in accordance with that derived from 3D photogrammetric models, with the exception of the residual displacement at the base of the wall after the 520 kJ experiment, reaching 0.95 m measured from camera images versus 0.72 m measured from photogrammetry (Table 2). This discrepancy is attributed to the rotation of the base block observed for this impact, having in mind that the video pointing method measures the maximal displacement of the block.

The maximal and residual values are reached later at top than at the base, and later during the second experiment than during the first one. During first and second experiment,

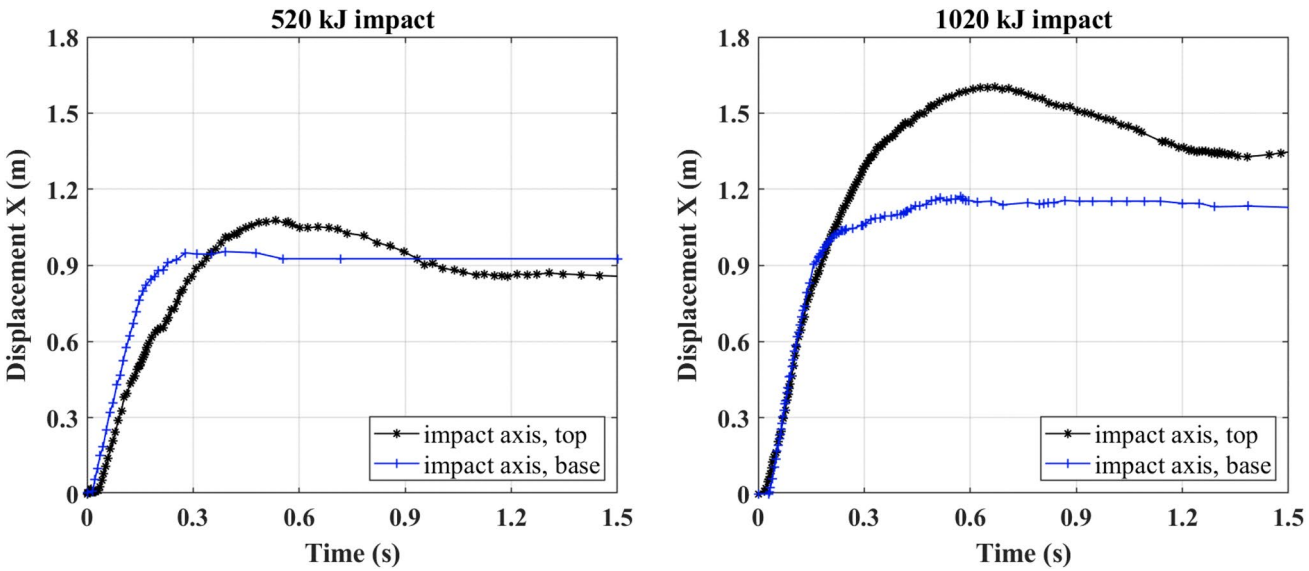

Fig. 7 Wall displacement with time at impact axis derived from high-speed camera Images. Base and top displacement during a) the 520 kJ impact experiment and b) during the 1020 kJ impact experiment (right)

Table 3 Displacement at impact axis along the X-axis measured from high-speed camera images (m)

Impact	Maximal		Residual		Reversible	
	Base	Top	Base	Top	Base	Top
1: 520 kJ	0.95	1.08	0.93	0.85	0.02	0.32
2: 1020 kJ	1.17	1.60	1.13	1.36	0.04	0.24

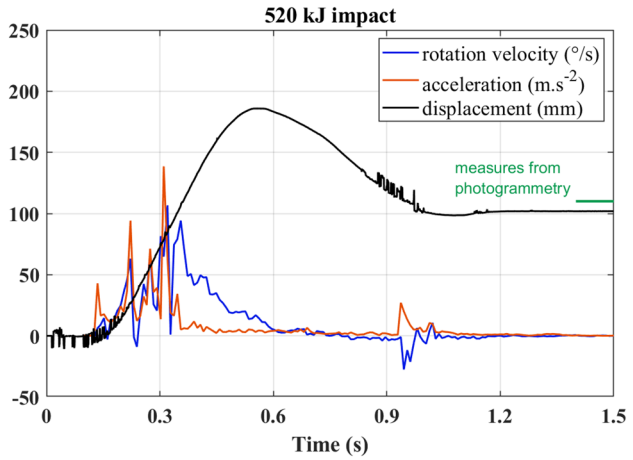

Fig. 8 Measurements in the distant plane and 2.8 m from the ground (point D)

the maximum displacement at the wall top is reached at $t = 0.55$ s and 0.70 s, respectively, and the residual displacement is reached after 1.10 s and 1.20 s respectively. Most of the reversible displacement is attributed to the tilting back of the wall on its back edge.

The real-time displacement in the distant plane being not measurable thanks to the video, measures during the first experiment came from cable position sensor located at point D are plotted Fig. 8, together with the acceleration and rotation velocity. Displacement occurs with a time lag as large as 0.15 s after the impact beginning, and reaches a maximum value of 0.185 m at $t = 0.55$ s. A significant reverse displacement is observed, leading to a residual displacement of about 0.100 m, in consistency with the measure derived from photogrammetry. The acceleration and rotation speed at the same point exhibit peak values exceeding 140 m/s^2 and 100°/s, respectively, reached at $t = 0.3$ s approximately. While the acceleration drops after the peak is reached, the rotation decreases progressively and reaches zero when displacement is maximum ($t = 0.55$ s). These curves highlight that the displacement on the distant plane is delayed by 0.15 s with respect to that in the impact axis, it involves a significant tilting that is simultaneous to translation, and includes a reverse displacement exceeding 40% of the maximal displacement.

4 Numerical Model

Similarly, as for many fields of geotechnics, rockfall protection structures may be modeled using continuous modeling approaches, including the finite element method (FEM) and the finite difference method (FDM), or using discrete elements methods approaches (DEM). For instance, flexible barriers have been modeled using DEM (e.g., Dugelas et al. 2019) as well as FEM (e.g. Mentani et al. 2016). Embankments have been modeled using FEM (e.g. Ronco et al. 2009; Korini 2021), DEM (Plassiard and Donze 2009; Oggeri et al. 2021) as well as a FDM–DEM coupled approach (Breugnot et al. 2016). Concrete walls exposed to boulder impacts have mainly been modeled using FEM (Lam et al. 2018; Yong et al. 2019).

4.1 General Representation

The software FLAC3D based on an explicit finite volume formulation was used to model the wall and each of its components in a realistic way (Fig. 9). This software is well adapted for dynamic and large displacements and to model distinct elements, including linear structural element.

The blocks, the base, and the projectile, hereafter referred to as volume elements, were modeled with continuous materials. The concrete blocks were modelled using distinct volume elements, linked to each other by means of the FLAC3D piles elements. The blocks were stacked as in the studied wall. The wall was placed on an elastically deformable base. The volume elements interacted with each other through interface elements which permit contact detection and forces transfer from one volume element to the other. The mesh size was set to 200 mm for blocks and projectile and 400 mm for the base that is small enough to ensure a good description of the final deformation of the wall without generating unrealistic stress and strain in the zones. It was verified that the zones dimensions do not influence significantly the structure global behavior.

Modeling of the various elements, their non-linear mechanical behavior and their interactions allows us to account for as much as possible of the different energy dissipation mechanisms activated during impact. This is of paramount importance when dealing with a structure where impact response, notably in terms of displacement,

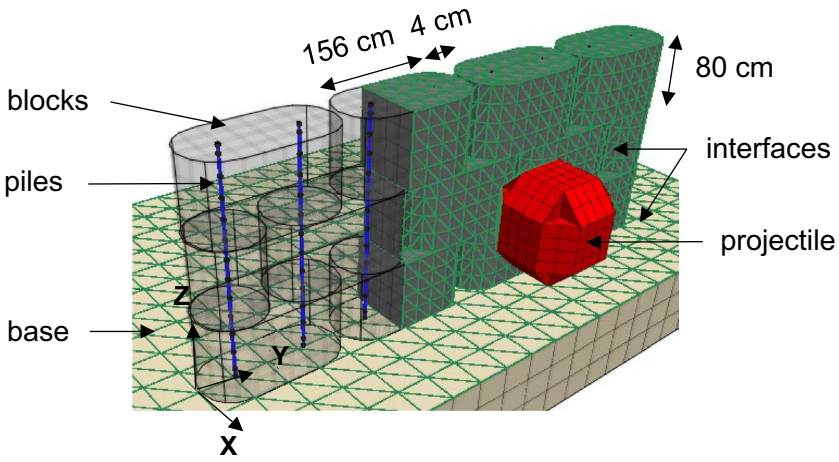

Fig. 9 FLAC3D model of the structure: blocks are modeled as continuum and interact with each other thanks to interfaces and are interconnected using structural elements (illustrated here for a linear wall)

is associated with energy transfer and dissipation. This is also necessary to ensure the model robustness and to obtain relevant data associated with physical mechanisms.

4.2 Volume Elements

The blocks are parallelepiped shaped volume elements with rounded vertical edges whose dimensions are close to that of the real blocks to the centimeter. Thanks to the space left between blocks due to the rounding of vertical edges, the contacts between blocks are limited in the model (as is the case with the real wall).

The base, modeling the ground supporting the wall, is designed to reproduce the interactions between the wall and the soil during the displacement of the wall: local indentation and friction. Particular attention was paid to the base model, to avoid any adverse interaction feedback on the wall, for example due to the reflection of compression waves at the base boundaries. The base was a rectangular parallelepiped with 1.5 m overhangs in front and on the sides of the wall and 3.0 m behind the wall to maintain a substantial overhang after the wall has been deformed. The height of the base was fixed to one meter.

The geometry of the projectile was chosen to best represent the real projectile used. Nevertheless, some simplifications were made concerning corners to avoid numerical problems during the wall/projectile contact due to the geometry of the zones in the corners (Fig. 2).

The mesh was chosen relatively large to maintain an affordable computation time (10 h for a 1 s simulation with a PC: Intel®Core™ i7-6700 K CPU @4.00 GHz, 32 Go de RAM).

The concrete blocks were associated with the *"Mohr–Coulomb"* elastoplastic constitutive law in FLAC3D. This law gives the following Mohr–Coulomb failure criterion (Eq. 1) and a tension cutoff criterion (Eq. 2):

$$f^s = -\sigma_1 + \sigma_3 . N_\Phi - 2.C.\sqrt{N_\Phi} \tag{1}$$

$$f^t = \sigma_3 - \sigma^t_{\max}, \tag{2}$$

where σ_1 and σ_3 are the principal stresses, C is the cohesion, and N_Φ is a function of the friction angle Φ such that.

$$N_\Phi = \frac{1+\sin(\Phi)}{1-\sin(\Phi)}, \tag{3}$$

$\sigma^t_{\max}$ is the tensile strength applied in the model given by

$$\sigma^t_{\max} = \max\left(\frac{C}{\tan\Phi}; \sigma^t\right), \tag{4}$$

where σ_t is the tensile strength.

In the elastic domain, the Hooke's relation is applied between the stresses and deformations as a function of the Young's modulus E and the Poisson ratio ν. When the plastic domain is reached, resulting from shear or tension failure, the principal stresses are determined using either a non-associated flow rule involving the dilation angle ψ (for shear) or an associated flow rule (for tension). This constitutive law is a simple method of describing the behavior of concrete while considering the plastic deformation of the blocks. The material behavior is not described with a complex model, but the way the energy dissipation and force transfer modification associated with plasticization are accounted for is considered precise enough to describe the overall behavior of the structure.

The base and projectile were associated with an elastic constitutive law. Indeed, during the experiments, neither the compact ground supporting the wall nor the projectile exhibited significant damage.

The numerical parameters of the Mohr–Coulomb constitutive law selected for the concrete blocks (Table 4) were determined from both literature data (i.e., Poisson ratio and dilation angle) and characterization tests on concrete

Table 4 Volumetric elements constitutive laws and parameters

Parameter	Blocks	Base	Projectile
Density (kg/m^3)	2100	2500	2656
Constitutive law	Mohr–Coulomb	Elastic	Elastic
Young modulus (Pa)	1.1×10^{10}	5.5×10^{9}	2.2×10^{10}
Poisson ratio (–)	0.2	0.2	0.2
Tensile strength (Pa)	4.1×10^{6}	–	–
Cohesion (Pa)	7.0×10^{6}	–	–
Friction (°)	57	–	–
Dilation angle (°)	0	–	–

samples. The Mohr–Coulomb parameters of the failure envelope (cohesion and friction) were defined using the experimental value of the compressive strength (σc), obtained from simple compression tests and the tensile strength (σ_t) obtained from splitting tensile strength tests (Brazilian test). The value of σ_t is increased by 0.3 MPa to take into account the rebars. In the end, the values given to σ_t and σ_c are 4.1 MPa and 48 MPa, respectively, resulting in a 7 MPa cohesion and a 57° friction angle. In addition, simple compression tests provided the concrete blocks Young modulus.

The Young modulus for the base is supposed to be twice lower than that of the block's Young modulus, while the Young modulus for the projectile is twice as high. The block density was defined so that the mass of the block equals the mass of the real blocks, to compensate the difference in volume between the real and the modeled blocks, these latter having no reservation.

4.3 Interfaces

FLAC3D interfaces managing contacts between volume elements allowing sliding, detachment and force transfers were used in the model. Interfaces are necessary for the contacts between volume elements to be detected. With FLAC3D, the contact between two volume elements is managed via the interfaces and is governed by normal and tangential stiffness, a Mohr–Coulomb failure criterion characterized by the cohesion and the friction angle at the interface (Fig. 10a). A tensile failure criterion, a shear failure criterion as well as an expansion angle can also be defined.

Interfaces were created on all faces of the blocks, at the base surface and on the projectile faces entering into contact with the wall.

Three different contact types were considered in the model (Fig. 10b), in accordance with the possible contact situations during the simulation. Each contact type associates the interface of a given type of object to the interface of another type of object. Normal and shear interaction forces are calculated at the interface nodes before being distributed to the nodes of the concerned zone of each volume element according to a mass weighting.

Since the interfaces were defined to model rigid and purely frictional contact between distinct objects, the cohesion was set to zero and a realistic friction value was considered. High values of normal and tangential stiffness were considered to permit contact between the elements with a limited influence of the elastic strain of the interfaces. As proposed by the software editor (Itasca Consulting Group Inc. 2019), the stiffness values were defined using the following criterion, which is relevant for rigid contacts between volume elements:

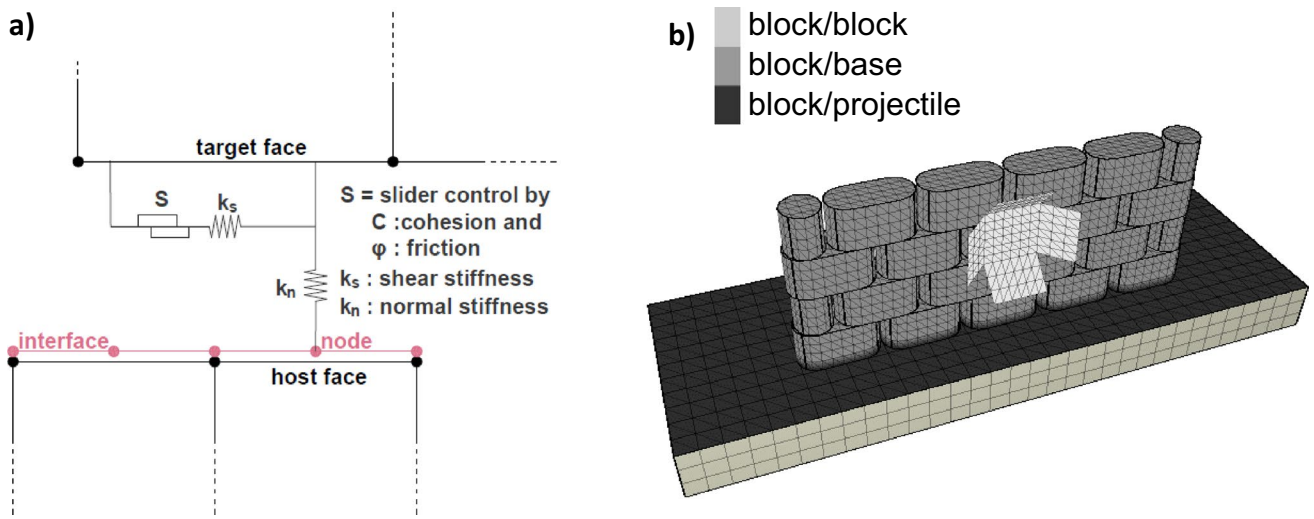

Fig. 10 Interfaces: model managing the contact between volume elements (**a**) and the three contact types considered in the model (illustration for a linear wall) (**b**)

Table 5 Interfaces parameters

Parameter	Block/block	Block/slab	Block/projectile
Normal stiffness (Pa/m)	6.1×10^{11}	6.1×10^{11}	1.9×10^{12}
Shear stiffness (Pa/m)	6.1×10^{11}	6.1×10^{11}	1.9×10^{12}
Friction (°)	23°	22°	22°

$$k_{\text{criterion}} = 10.\max\left(\frac{K+4/3G}{\Delta z\text{min}}\right), \tag{5}$$

where K and G are the bulk and shear modulus of materials in contact and Δzmin is the smallest dimension in the normal direction of the two zones in contact.

As for the friction angle between two blocks, a value of 31° was obtained by a static measure at the interface. To take into account the dynamics, a reduction of 25% was applied to the static value to obtain the numerical interface friction value of 23° (Table 5). In the absence of specific measurement, the dynamic friction angle for the block–slab and projectile–block interfaces were assumed to be 22°. It will be seen that friction at the base is not the prevailing mechanism in the structure response, suggesting that uncertainty in the friction angle does not affect the study results (Fig. 17).

4.4 Structural Elements Assembly

The metallic reinforcements of the structure were modeled using available FLAC3D linear structural elements. This type of element allows us to model structural elements which interact with zones of the volumetric elements via nodes.

The metallic reinforcements were modeled by "pile" elements (Fig. 11a). These constant cross-sectional (A) elements combine an elastic compressive behavior (Fig. 11b), a resistance to flexion describing variable cross-sectional geometry specified by users through second moments of inertia I_y and I_z, a polar moment J, an elastic–plastic behavior in tension based on the tensile yield strength (F_{ty}) and the tensile failure strain (ε_{tf}) of the element in addition to its Young's modulus (E).

The combination of the sling and the tubes passing through the vertical holes of the stacked blocks is modeled by one pile element. The pile element characteristics were defined in view to model the mechanical contribution of these combined elements on the structure response. Elements were created from bottom to top of the wall at their real position in the real wall (Fig. 12a).

These structural elements transmit forces from one block to the other. The free space between the tubes and the blocks is a key parameter in the dynamic response of the wall. This free space, thereafter referred to as mechanical play, is accounted for in the simulation via a specific structural element–block interaction model: each node of a pile element is initially free to move in all three directions until its transverse displacement equals the play existing between the tube and the block. Then the transverse displacement (y_b, z_b) of the node with respect to the block (zone) is blocked. The experimental value of 7 mm was used. To consider the vertical slack at the top of the wall induced by the smooth connection between slings and the continuous head cable, a free displacement of 20 mm was considered at the top of the wall.

Parameters of the pile elements were determined in accordance with the characteristic of the reinforcement metallic elements to best represent the combination of a sling inserted in a succession of tubes (Table 6). The tubes were considered for setting the shear and flexural strength of the pile elements, while considering the characteristics of the slings to determine the tensile strength and critical deformation characteristics (Young modulus, ultimate tensile failure deformation) of the pile.

4.5 Base Boundary Conditions

To limit reflection of elastic waves within elastic volumetric elements of the base, the so-called "quiet" condition

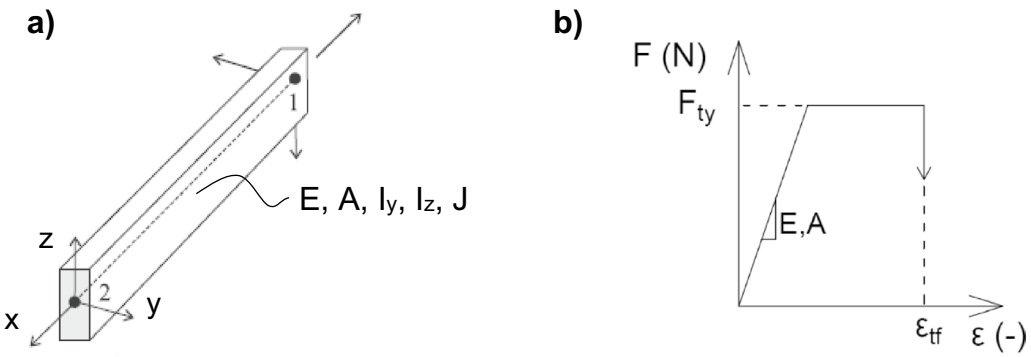

Fig. 11 Pile element **a** parameters describing the flexional and axial behavior of the linear element, **b** tensile elasto-plastic behavior

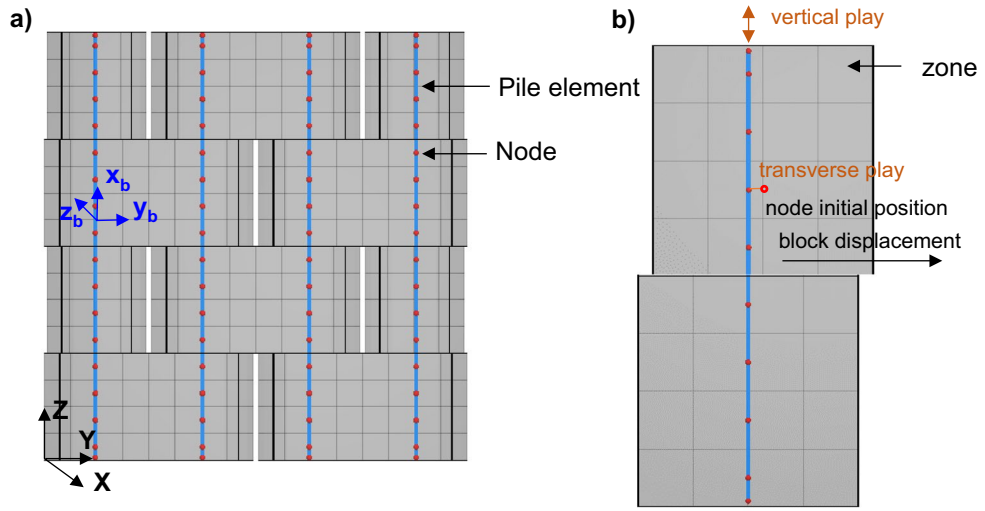

Fig. 12 Structural elements/blocks interaction model. **a** Front view: piles crossing the wall over the entire height, **b** cross-sectional view: node to zone contact and introduction of limited free displacement (mechanical play) existing in the structure

Table 6 Pile parameters

	Tubes	Sling
Density (kg/m^3)	7500	/
Young modulus (Pa)	/	1.6×10^{11}
Poisson ratio (–)	0.3	/
Section (m^2)	3.3×10^{-3}	/
Tensile strength (N)	/	4.4×10^{5}
Tensile limit failure deformation (–)	/	0.22
Second moment y (m^4)	7.2×10^{-6}	/
Second moment z (m^4)	7.2×10^{-6}	/
Polar moment (m^4)	1.4×10^{-5}	/

available in FLAC3D was imposed on the lateral sides and on the bottom surface of the base (Fig. 9). The calculation procedure consists of applying external forces on boundary nodes compensating the static loads in lieu of imposing fixed displacements on the nodes. When reaching the boundaries, displacements are damped by viscous forces applied on the nodes that avoid the inward reflection of elastic waves.

4.6 Simulation's Procedure

The numerical model was used to define the zigzag wall geometry and to simulate these full-scale impact experiments presented in Table 1. Firstly, the wall and the base were created and the static gravitational equilibrium was reached. Then, the dynamic loading was imposed. Impacts were simulated by throwing horizontally the projectile on the wall with a given initial velocity. The conditions were similar to experimental conditions regarding the projectile geometry, mass, velocity magnitude and pre-impact trajectory.

No artificial damping was considered in the simulations, except for the viscosity applied in quiet boundaries.

5 Comparison Between Numerical and Experimental Results

Comparison between numerical and experimental results will focus on residual and dynamical displacement. The plasticization of the blocks is also studied in comparison with experimental observations. The comparisons will evaluate the ability of the model to reproduce the displacement behavior of the walls and the capacity of the numerical model to integrate the main physical phenomena involved during impact.

The global deformations of the walls in the simulations are very similar to those observed experimentally for the two tested impact energies. The length of the wall that experienced a significant displacement during impact and the trends concerning rotation and translation of the blocks are well reproduced (Fig. 13a and c). A rather good global agreement is observed in terms of displacement with time of the top of the wall, for the two impacts (Fig. 13b and d). This in particular concerns the wall velocity before reaching the maximal displacement and the time delay before to observe displacement of the blocks on the distant plane. This suggests that the mechanisms governing force transmission within the walls, including the influence of the mechanical plays, are well taken into account in the numerical model.

Similar values of uplift of the wall are observed with a slight overestimation by the model (Fig. 14b). On the contrary, the model fails to reproduce the wall reverse displacement related to the tilting of the wall (Fig. 13b and b).

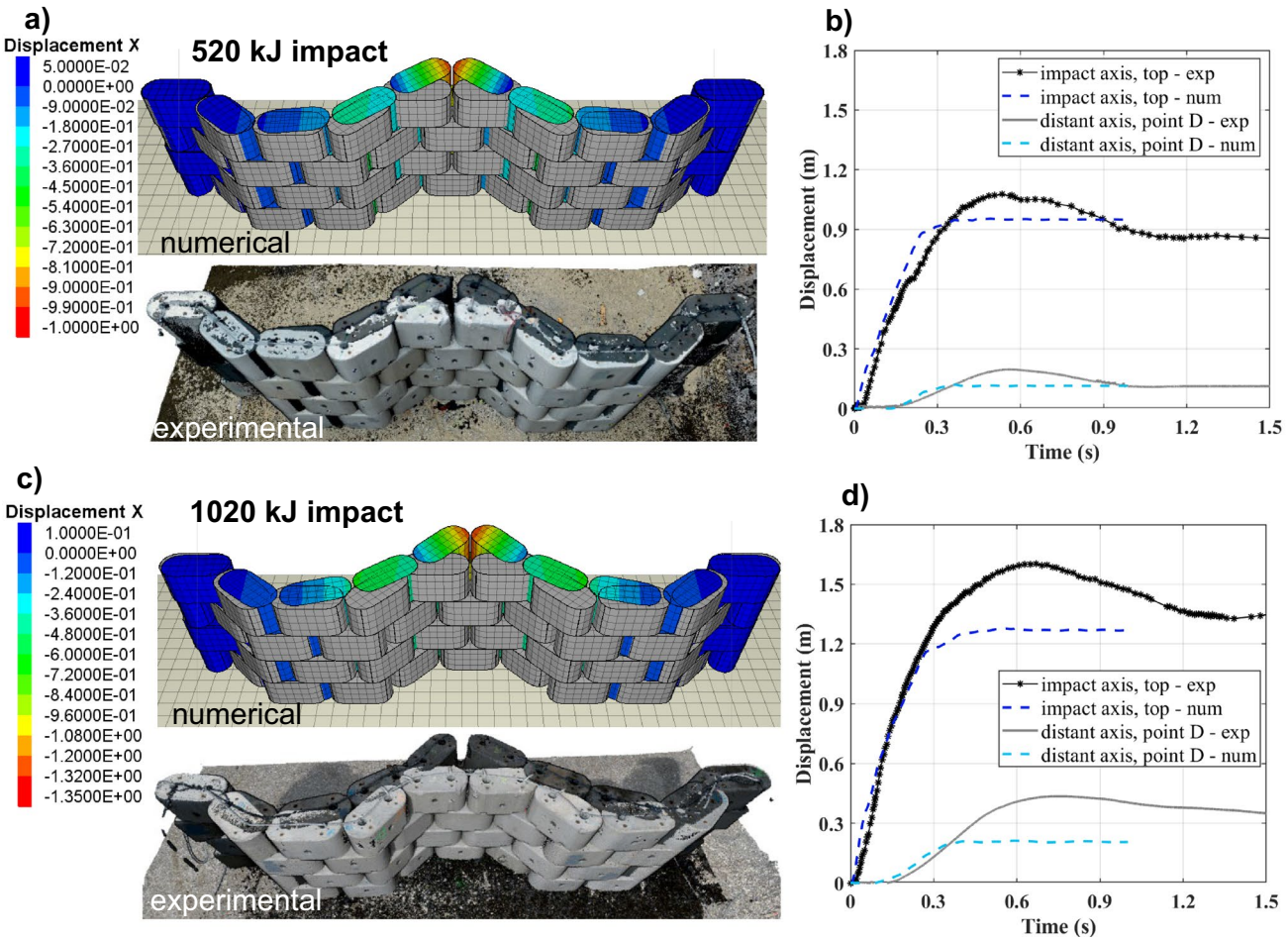

Fig. 13 Numerical vs experimental results for the first (top) and second impact experiments (bottom). Superimposed views showing the whole structure deformation (left) and displacement at the top of the wall (right)

It can be seen from Fig. 14 that the model efficiently predicts the residual displacement at the base for the two impact tests. At the top of the walls, the residual displacement is slightly overestimated for the 520 kJ impact experiment and underestimated for the 1020 kJ impact experiment.

In conclusion, the results show that the numerical model, accounting the majority of the phenomena involved under impact such as sliding at base, uplift of the wall, relative displacement between blocks and the force transmission kinematic allows to reproduce the response of the walls under impact regarding dynamic and residual displacement.

The numerical model considers the blocks as unbreakable entities, where damage is modeled through an elastoplastic constitutive law, which considers shear and tension plastic deformation of the material. The plasticization pattern observed in the simulations exhibits very similar trends as that observed after the two experiments (Figs. 15 and 16). This first concerns the impacted block which experiences high level of damage as well as the blocks in the impact vicinity, in particular during the 1020 kJ impact experiment. Local damage observed at distance from the impact axis, resulting from friction at the contact points between blocks, is also observed in the simulations.

In the end, the whole results of the numerical model, both for 520 kJ and 1020 kJ impacts, were in excellent agreement with the experimental results. Similar global kinematics and final state of the walls are observed between the simulations and the experiments. The main difference concerns the reversible displacement observed at top of the wall, that is almost absent in the simulations.

Supplementing the results obtained at the reduced scale (Furet et al. 2020), these results ensure the robustness of the model that will be used to optimize the design of protection structures.

The mid-term aim with this numerical model is to design structures studying the general stability of structures with respect to overturning and predicting the wall displacements. In order to provide recommendations for the design of this kind of walls protecting infrastructures, the model represents an effective tool to lead future specifics studies varying

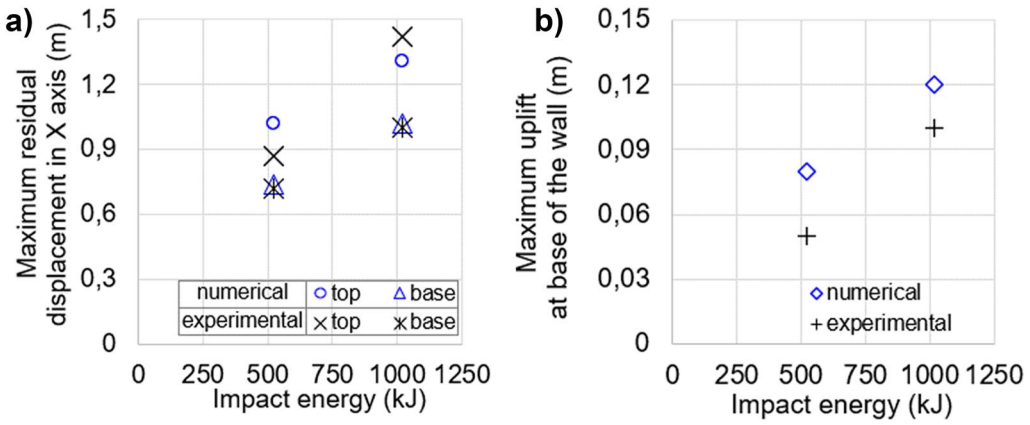

Fig. 14 Numerical vs experimental results for the two impacts: **a** maximum residual displacement of the wall in the X-axis direction and **b** maximum uplift of the wall base

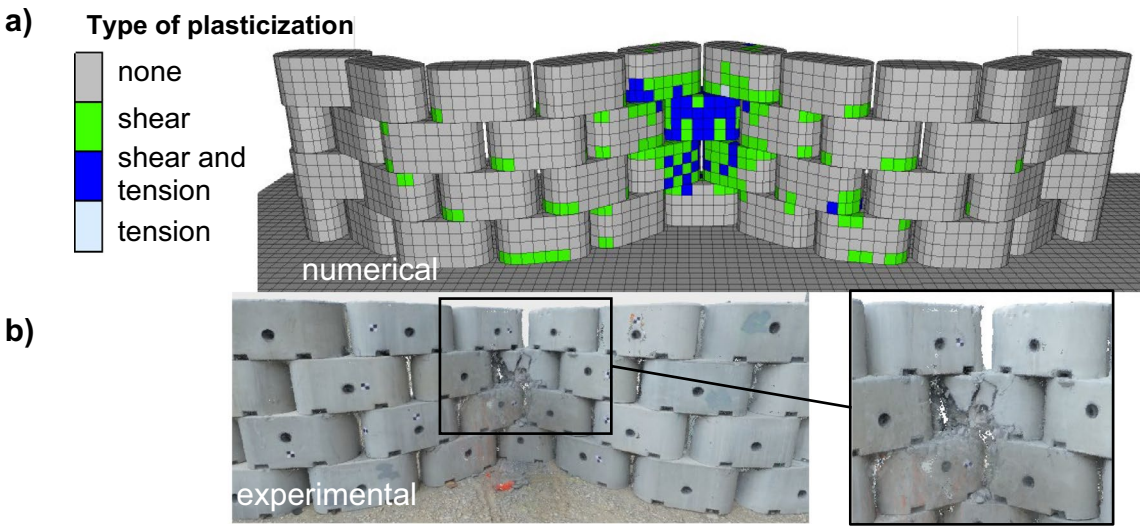

Fig. 15 Wall damage after the 520 kJ impact **a** zones plasticization observed from the simulations, **b** view of the wall and focus on the impacted area

(i) the structure design (play between tube and block, wall geometry…) and (ii) the impact conditions (impact location, kinetic energy…).

6 Discussion Concerning Energy Dissipation

As dealing with a structure exposed to impact, energy dissipation is a key issue to address. Identifying the dissipation sources and quantifying their respective contribution is thus a prerequisite for structural improvement. Numerical model made it possible to highlight complex mechanisms that were not possible to experimentally determine. The following paragraphs presents the physical phenomena possibly involved in the energy dissipation and then the partial energy balance calculated in the numerical model.

6.1 Energy Dissipation Phenomena on the Walls

Dissipative mechanisms play a significant role in the structure response and contribute to its efficiency in withstanding the impact. Indeed, many sources of energy dissipation are activated in the structure when subjected to impact. The damage of the block dissipates energy mostly by plastic deformation of the material and marginally by fracturing, phenomenon that is not very efficient in dissipating energy (Guccione et al. 2021). During the displacement, contacts between the elements dissipate energy by friction. In particular, relative displacement between the different blocks, the base and the projectiles are susceptible to dissipate energy. Energy could be stocked in the metallic elements or dissipated when plasticization is observed. Moreover, energy could be propagated by elastic waves or retained

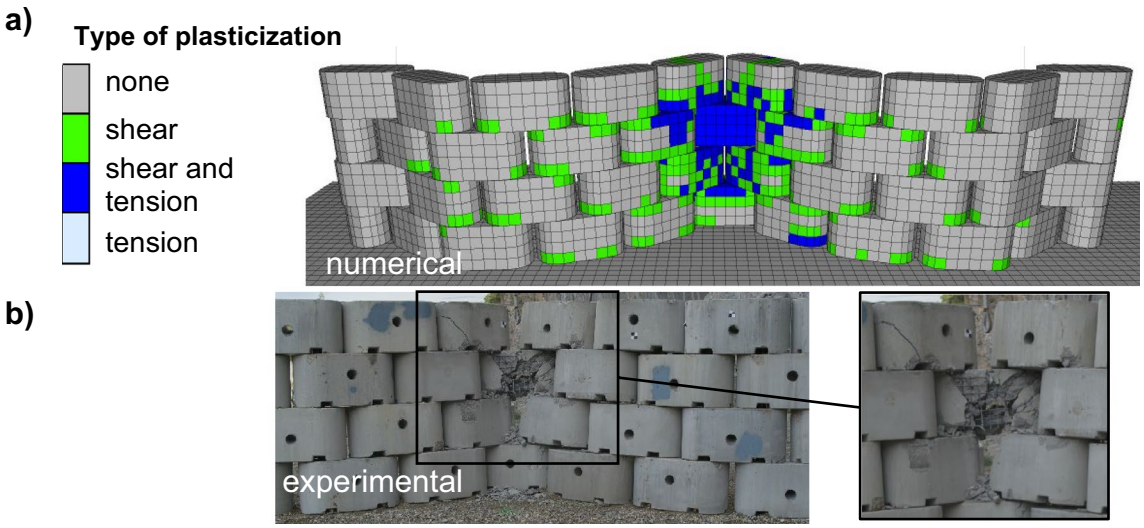

Fig. 16 Wall damage after the 1020 kJ impact **a** zones plasticization observed from the simulations, **b** view of the wall and focus on the impacted area

as kinetic energy by the projectile. During the full-scale tests and in the numerical simulation, the projectile kinetic energy after impact is not significant compared to the one before impact (Furet et al. 2020).

Estimating the energy dissipation from experimental results is difficult because many sources of energy dissipation such as plastic damage or friction linked to small displacements are hardly accessible. Numerical models represent a good way to access to specific results and calculate energy dissipation. For the purpose of this study, the calculations were focused on energy dissipated within and between each structure elements. In particular cumulative values of the energy dissipated with time by friction and plasticization were computed. The total plastic work dissipated during each time step is calculated in FLAC3D using total and elastic deviatoric work estimated thanks to shear strain and stress of the zones (Itasca Consulting Group Inc. 2019). To calculate energy dissipation by friction, specific functions are developed using the Fish language integrated into the FLAC3D software where shear forces and displacements at interfaces nodes are used. Energy dissipated is calculated cumulating the friction at nodes as follows:

$$E_{fric} = \sum_{t0}^{t\text{final}} \sum_{\text{node}i} \Delta E_i, \tag{6}$$

where

$$\begin{aligned} \Delta E_i = & \frac{(Fs_x(t-1) + Fs_x(t))}{2}.(ds_x(t) - ds_x(t-1)) \\ & + \frac{(Fs_y(t-1) + Fs_y(t))}{2}.(ds_y(t) - ds_y(t-1)) \\ & + \frac{(Fs_z(t-1) + Fs_z(t))}{2}.(ds_z(t) - ds_z(t-1)). \end{aligned} \tag{7}$$

With Fs_x, Fs_y and Fs_z expressing the instantaneous shear force component, respectively, in X, Y and Z axis and ds_x, ds_y et ds_z expressing the cumulative shear displacement component, respectively, along the X, Y and Z axes.

t expresses the current time step and t–1, the previous time step, considered for the calculation. As the functions are not called at each time step of the simulation, this latter time steps differ from the simulation time steps.

6.2 Energy Dissipation Balance in the Simulations

Evolution in time and proportion relatively to impact kinetic energy is rather similar for the two impacts (Fig. 17). Indeed, displacements of the wall allow to dissipate significant amount of energy which increases with the intensity of the solicitation. The same observation is true for plasticization, and the energy dissipated by plasticization increases with the impact kinetic energy, even if the areas of the wall where plasticization occurred are similar for the two experiments.

Accounting for the similarity between the two experiments, results are detailed for the second impact test only. At the end of the second experiment, the energy dissipated by friction amounts to 232 kJ. In detail, friction

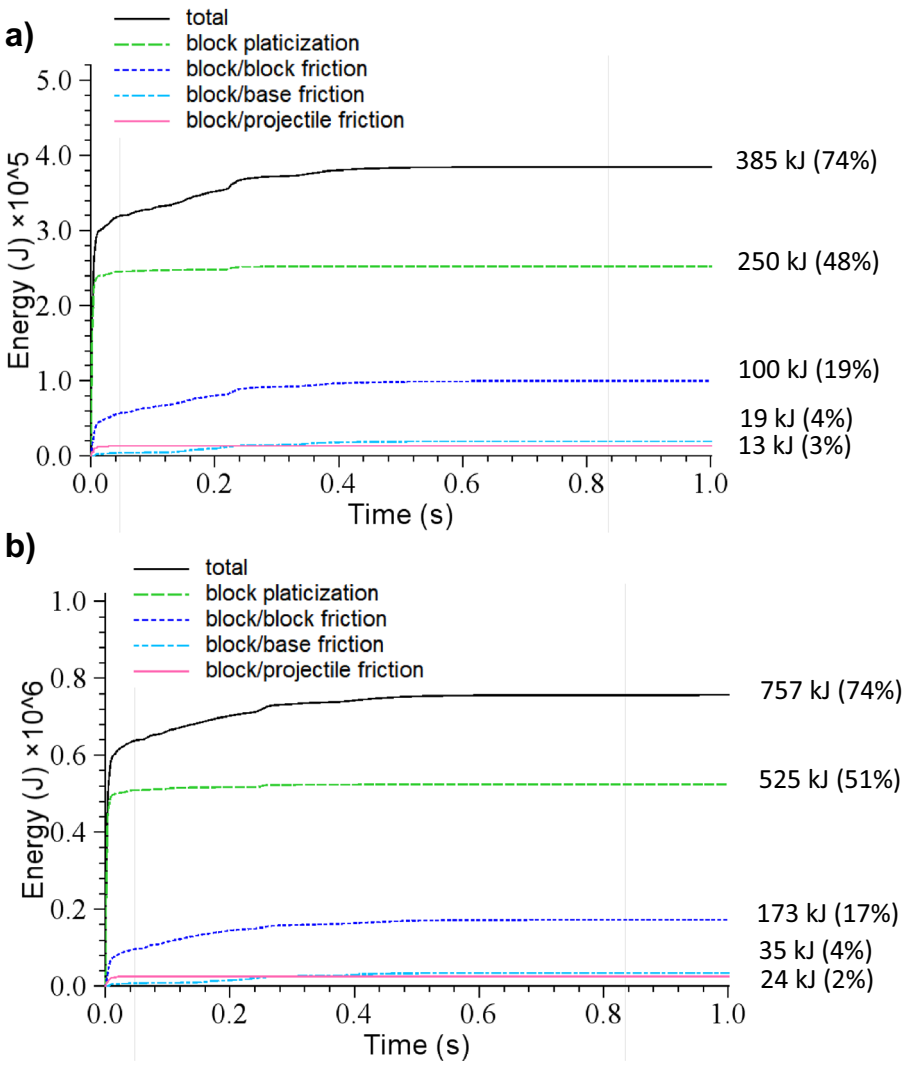

Fig. 17 Evolution with time, final value (kJ) and ratio with respect to the impact kinetic energy (%) of the energy dissipated by various mechanisms during the 520 kJ impact (top) and the 1020 kJ impact (bottom)

dissipates 24 kJ between the projectile and the wall, 35 kJ between the wall and the base and 173 kJ between blocks (Fig. 17b). The plasticization of the blocks dissipates about 525 kJ (Fig. 17b). In total, damage and friction dissipate 74% of the impact energy. The rest of the energy (26%) is presumed propagated or dissipated via phenomena that are difficult to quantify with FLAC3D (deformation of structural elements, propagation by elastic waves, dissipation by quiet conditions viscosity, fracturing). The proportion of energy dissipated by plastic deformation, of the order of 50%, is lower than that for reinforced embankments where the dissipation by compaction of soil reaches 75–80% of the impact energy (Ronco et al. 2009; Kister and Fontana 2011). In articulated walls, a significant part of the energy (20%) is dissipated by friction between blocks and between the structure and the base.

The evolution with time of the total energy dissipated shows a fast increase from the very beginning of the impact, up to 10 ms, then a gradual low increase until stabilization, after 500–600 ms (Fig. 17). In accordance with the dynamic response of the walls, the dissipative mechanisms are mobilized at different times. The first contribution results from the plasticization of the impacted concrete block. The second contribution is due to friction between projectile and impacted block and in a greater magnitude between blocks of the structure which is initiated after a few ms. Friction at the base is activated later, from about 20 ms when blocks at the wall base start sliding. Significant dissipation by plasticization and by friction is observed up to 300 ms after the impact beginning.

7 Conclusions

This article has presented real-scale experiments and numerical simulations of impacts on 1.9 m wide zigzag protective walls against rockfall made of concrete blocks articulated through metallic elements.

Two impacts with a kinetic energy of 520 kJ and 1020 kJ were performed horizontally at the centers of the walls. The experiments showed this technology is efficient to intercept rock impacts up to 1000 kJ. Measurement allowed to highlight the dynamic response of the walls when impacted. The impacted blocks are displaced quickly under impact (Fig. 10) and thanks to the elements connecting the blocks, the distant components of the structure were displaced as well, with a certain time delay due to the play existing between the structural elements (Fig. 12). At impact axis, on a length of four blocks, the walls were uplifted and tilted on the rear edge when the sliding stopped. Reversible displacement was measured, with small amplitude at base of the walls and significant amplitude at top. After impact, blocks walls are significantly displaced under a length exceeding six blocks and damaged locally near the impact location (Figs. 8 and 9).

In comparison with the experimental results, the original model developed with FLAC3D showed a good capacity to reproduce the response of the walls for the two impacts. The residual displacements of the entire wall are in very good agreement with the experimental results. The numerical results attested to a good description of the dynamic behavior of the wall under impact both concerning the time before to reach the maximal displacement and the time delay observed before the displacement of the blocks in the distant plane. The choice to model accurately the different components and the complex interactions between them existing in the technology allowed to reproduce the dynamic response of the structure taking into account the physical phenomena involved during the impact. Thus, the model could be used to discuss the energy dissipation phenomena existing in the walls during impact. For the 1020 kJ impact results showed that the plasticization of the concrete blocks dissipates 51% of the kinetic impact energy. Friction dissipated 23% of the kinetic impact energy with a major fraction due to friction between blocks (17%). A majority of the energy dissipated by plasticization is dissipated before 0.01 s after impact beginning while the friction dissipated energy for 0.6 s after the impact beginning. These results are in accordance with the localized plasticization of the blocks, observed experimentally and reproduced in the model and the displacement time duration of the blocks of the walls.

The experiments performed at real-scale have proved that low footprint walls made up of articulated concrete blocks are efficient means to intercept rockfall with kinetic energy up to 1000 kJ, which is considered as a high value for a wall. A numerical model of the technology allowing to simulate impacts on walls has been developed. The model was validated by confrontation of the numerical results with experimental data resulting from a large number of measurements deployed during experiments. By identifying energy dissipation phenomena and calculating their proportion relatively to the kinetic impact energy, the numerical model allowed us to better understand the role of each component in the structure. The numerical model represents a robust tool to both optimize the technology by studying the influence of characteristics such as plays amplitude between elements and optimize the design of protective structures under impact.

Acknowledgements The authors would like to thank Patrick Joffrin and Christophe Pruvost from the Université Gustave Eiffel, Jérome Gineys from Cerema for their technical assistance conducting the experiments, the partner Myotis for the acquisition of some of the experimental data and Julien Lorentz from Géolithe Innov for his investment leading the experiments. The authors express their appreciation to Itasca and more specifically to Marco Camusso for the personal help they benefited from the Itasca Educational Partnership.

Funding This work was conducted as part of the C2ROP French national project and a Cifre thesis. It also benefited from a financial support from the Auvergne Rhône-Alpes region.

References

Breugnot A, Lambert S, Villard P, Gotteland Ph (2016) A discrete/continuous coupled approach for modeling impacts on cellular geostructures. Rock Mech Rock Eng 49(5):1831–1848. https://doi.org/10.1007/s00603-015-0886-8

Colgan T, Ewe E (2019) Design of a large scale rockfall protection bund for coastal transport corridor recovery following the 2016 Kaikōura earthquake in Pacific. In: conference on earthquake engineering. Auckland, New Zealand

Dugelas L, Coulibaly JB, Bourrier F, Lambert S, Chanut MA et al (2019) Assessment of the predictive capabilities of discrete element models for flexible rockfall barriers. Int J Impact Eng 133:1–15. https://doi.org/10.1016/j.ijimpeng.2019.103365

EOTA (2018) Falling rock protections kits. European Assessment Document. EAD 340059-00-0106/c 417/07

Furet A (2020) Modélisations expérimentale et numérique d'ouvrages pare-blocs modulaires: application à la technologie Bloc Armé®. Université Grenoble Alpes, Français

Furet A, Lambert S, Villard P, Jarrin J-P, Lorentz J (2020) Réponse sous impact de murs pare-blocs. Rev Fr Géotech 163:9. https://doi.org/10.1051/geotech/2020017

Green R, Finlan JS (2021) Rapid design of a modular rockfall protection wall in response to the 2016 KaiKoura earthquake. GeoExtreme 2021:151–165. https://doi.org/10.1061/9780784483688.015

Guccione DV, Thoeni K, Fityus S, Nader F, Giacomini A, Buzzi O (2021) An experimental setup to study the fragmentation of rocks upon impact. Rock Mech Rock Eng. https://doi.org/10.1007/s00603-021-02501-3

Hara T, Tsuji S, Yoshida M, Ito S, Sawada K (2012) Experimental development of new type reinforced soil wall. Int J Geomate 2(2):213–218

Hearn G, Barrett R, Henson H (1996) Development of effective rockfall barriers. Transp Res Rec 1504:1–11

Itasca Consulting Group, Inc. (2019). FLAC3D - Fast Lagrangian Analysis of Continua in Three Dimensions, Ver. 7.0., Minneapolis

Kister B, Fontana O (2011) On the evaluation of rockfall parameters and the design of protection embankments – a case study in interdisciplinary workshop on rockfall protection – Rocexs, Innsbruck, Austria, 31–32

Korini O (2021) Comportement et dimensionnement aux impacts des merlons de protection en sol renforcé par géosynthétiques. Ecole Doctorale Mecanique, Energétique, Génie Civil, Acoustique (MEGA)

Korini O, Bost M, Rajot JP, Bennani Y, Freitag N (2019) Experimental study of reinforced soil bunds subjected to horizontal impact in14th International Congress on Rock Mechanics and Rock Engineering (ISRM), Foz do Iguassu, Brazil

Korini O, Bost M, Rajot JP, Bennani Y, Freitag N (2021) The influence of geosynthetics design on the behavior of reinforced soil embankments subjected to rockfall impacts. Eng Geol. https://doi.org/10.1016/j.enggeo.2021.106054

Lam NTK, Yong ACY, Lam C, Kwan JSH, Perera JS, Disfani MM, Gad E (2018) Displacement-based approach for the assessment of overturning stability of rectangular rigid barriers subjected to point impact. J Eng Mech. https://doi.org/10.1061/(ASCE)EM.1943-7889.0001383

Lambert S, Bourrier F (2013) Design of rockfall protection embankments: a review. Eng Geol 154(28):77–88

Lambert S, Kister B (2018) Efficiency assessment of existing rockfall protection embankments based on an impact strength criterion. Eng Geol 243:1–9. https://doi.org/10.1016/j.enggeo.2018.06.008

Lambert S, Heymann A, Gotteland P, Nicot F (2014) Real-scale investigation of kinematic response of a rockfall protection embankment. Nat Haz Earth Syst Sci 14:1269–1281. https://doi.org/10.5194/nhess-14-1269-2014

Lambert S, Bourrier F, Gotteland P, Nicot F (2020) An experimental investigation of the response of slender protective structures to rockfall impacts. Can Geotech J. https://doi.org/10.1139/cgj-2019-0147

Lorentz J, Jarrin J-P, Meignan L, Leroux Mallouf R. (2018) Bloc Armé© – Landslides passive protective structure. In: 4th International Symposium Rock Slope Stability, Chambéry, France, pp. 105–106

Mentani A, Giacomini A, Buzzi O, Govoni L, Gottardi G, Fityus S (2016) Numerical modelling of a low-energy rockfall barrier: new insight into the bullet effect. Rock Mech Rock Eng 49(4):1247–1262. https://doi.org/10.1007/s00603-015-0803-1

Oggeri C, Ronco C, Vinai R (2021) Validation of numerical D.E.M. modelling of geogrid reinforced embankments for rockfall protection. Geoingeg Ambient Mineraria 58(1–2):36–45. https://doi.org/10.19199/2021.163-164.1121-9041.036

Peila D, Oggeri C, Castiglia C (2007) Ground reinforced embankments for rockfall protection: design and evaluation of full scale tests. Landslides 4:255–265. https://doi.org/10.1007/s10346-007-0081-4

Peila D, Oggeri C, Castiglia C, Recalcati P, Rimoldi P (2002) Testing and modelling geogrid reinforced soil embankments subject to high energy rock impacts, Geosynthetics in 7th ICG, Delmas, Gourc & Girard (eds.)

Plassiard J-P, Donzé F-V (2009) Rockfall impact parameters on embankments: a discrete element method analysis. Struct Eng Int 19(3):333–341

Ronco C, Oggeri C, Peila D (2009) Design of reinforced ground embankments used for rockfall protection. Nat Haz Earth Syst Sci 9(4):1189–1199

Simmons M, Pollak S, Peirone B (2009) High energy rock fall embankment constructed using a freestanding woven wire mesh reinforced soil structure in the 60th Highway Geology Symposium. Buffalo, New York, pp 290–301

Yong ACY, Lam C, Lam NTK, Perera JS, Kwan JSH (2019) Analytical solution for estimating sliding displacement of rigid barriers subjected to boulder impact. J Eng Mech. https://doi.org/10.1061/(ASCE)EM.1943-7889.0001576